energies

MDPI

Article

Phenol-Formaldehyde Resin-Based Carbons for CO_2 Separation at Sub-Atmospheric Pressures

Noelia Álvarez-Gutiérrez †, María Victoria Gil †, María Martínez †, Fernando Rubiera † and Covadonga Pevida *,†

Instituto Nacional del Carbón, INCAR-CSIC, Apartado 73, 33080 Oviedo, Spain; noeag@incar.csic.es (N.A.-G.); victoria.gil@incar.csic.es (M.V.G.); mariamf.mmf@gmail.com (M.M.); frubiera@incar.csic.es (F.R.)

* Correspondence: cpevida@incar.csic.es; Tel.: +34-985-11-90-90 (ext. 319); Fax: +34-985-29-76-62

† These authors contributed equally to this work.

Academic Editor: Wei-Hsin Chen

Received: 16 December 2015; Accepted: 6 March 2016; Published: 11 March 2016

Abstract: The challenge of developing effective separation and purification technologies that leave much smaller energy footprints is greater for carbon dioxide (CO_2) than for other gases. In addition to its involvement in climate change, CO_2 is present as an impurity in biogas and bio-hydrogen (biological production by dark fermentation), in post-combustion processes (flue gas, CO_2-N_2) and many other gas streams. Selected phenol-formaldehyde resin-based activated carbons prepared in our laboratory have been evaluated under static conditions (adsorption isotherms) as potential adsorbents for CO_2 separation at sub-atmospheric pressures, *i.e.*, in post-combustion processes or from biogas and bio-hydrogen streams. CO_2, H_2, N_2, and CH_4 adsorption isotherms at 25 °C and up to 100 kPa were obtained using a volumetric equipment and were correlated by applying the Sips model. Adsorption equilibrium was then predicted for multicomponent gas mixtures by extending the multicomponent Sips model and the Ideal Adsorbed Solution Theory (IAST) in conjunction with the Sips model. The CO_2 uptakes of the resin-derived carbons from CO_2-CH_4, CO_2-H_2, and CO_2-N_2 at atmospheric pressure were greater than those of the reference commercial carbon (Calgon BPL). The performance of the resin-derived carbons in terms of equilibrium of adsorption seems therefore relevant to CO_2 separation in post-combustion (flue gas, CO_2-N_2) and in hydrogen fermentation (CO_2-H_2, CO_2-CH_4).

Keywords: CO_2 separation; adsorption; phenolic-resin; activated carbons

1. Introduction

The sustainable production of energy is currently a topic of extensive research with the aim of producing low carbon footprint processes and mitigating the CO_2 impact [1]. As a sustainable and clean energy source with minimal or zero use of hydrocarbons, hydrogen is a promising alternative to fossil fuels [2]. Hydrogen can be generated by thermochemical, electrochemical or microbial fermentation processes. Biological methods are preferable to chemical methods because they offer the possibility of using sunlight, CO_2 and organic wastes as substrates for environmentally benign conversions under moderate conditions [3]. The biological methods for generating H_2 include light-dependent methods, such as direct and indirect biophotolysis and photo fermentation; and methods not dependent on light, such as the dark fermentation process and bioelectrochemical systems (BES). Hydrogen production through dark fermentation has advantages over the other processes because it does not require the input of external energy and it offers the possibility of rapid scalability owing to its similarity to the well-known anaerobic digestion process [4]. In addition, bio-hydrogen production from anaerobic fermentation is linked to bio-methane generation since the process develops in two main stages. In the first stage acidogenic bacteria break down substrates into primarily H_2, acetic acid, and CO_2, and in

the second stage methanogenic bacteria convert acetic acid, H_2, and CO_2 to methane gas. The two reactions can be separated, at least partially, in distinct bioreactors placed in series. Both streams must be further purified to obtain bio-hydrogen and bio-methane with a high calorific value, appropriate for industrial applications [5]. Concentrations of H_2 of up to 30–70 vol% on average and of up to 45–80 vol% in the case of CH_4 on average can be achieved but the presence of CO_2 in both streams (20–70 vol%) is a nuisance and needs to be removed for further utilization of H_2 and CH_4 [6].

On the other hand, conventional energy production from fossil fuels is one of the main sources of anthropogenic CO_2. The separation of CO_2 from flue gas (post-combustion CO_2 capture), is very challenging given that it is at near atmospheric pressure and CO_2 only represents between 4 to 15 vol%, depending on the fuel used, and if dry or wet basis conditions are considered. However, the conditions required for CO_2 transport, storage or subsequent use as a chemical make a concentration step necessary to reach the set target of *ca.* 95 vol%.

Different technologies have been evaluated to separate CO_2 under sub-atmospheric pressure and particular emphasis has been paid in recent years to post-combustion CO_2 capture due to increasing concerns about global warming and climate change. Adsorption with low temperature solid sorbents has the potential to reduce the energy penalty associated with the separation of CO_2 at sub-atmospheric pressures, not only under post-combustion capture conditions (CO_2/N_2 separation) but also for bio-hydrogen (CO_2/H_2 separation) and bio-methane production (CO_2/CH_4 separation) [7,8]. However, the success of these approaches depends on the development of adsorbents with a high selectivity, sufficient adsorption capacity and easy regeneration. Carbon adsorbents fulfil all these requirements: they have a significant adsorption capacity at atmospheric pressure and the necessary characteristics for the separation of CO_2 at sub-atmospheric pressures including hydrophobicity, low cost and low intensity in terms of the amount of energy required for regeneration.

The distinction between activated or porous carbons and carbon molecular sieves has not been clearly defined. Whereas most of the pores in carbon molecular sieves are in the molecular size range, activated carbons may also have very small pores. The main difference is that activated carbons separate molecules through differences in their adsorption equilibrium whereas carbon molecular sieves provide molecular separations based on rate of adsorption, allowing the separation of molecules on the basis of their size, rather than on the differences in adsorption capacity [9,10].

The use of polymeric precursors to produce activated carbons allows the incorporation of custom tailored features (e.g., pore size, conformation, *etc.*) along with other material properties to meet the required specifications. Phenol-formaldehyde resin-derived microporous activated carbons have been previously studied in our laboratory [6,11,12]. They can be produced in a wide variety of physical forms, at a low cost and with a close control of porosity. More importantly, all these features are accompanied by a very low level of impurities and good physical strength, key parameter in the design of an adsorption process [13,14].

In this work, the performance of phenol-formaldehyde resin-based activated carbons prepared in our laboratory to separate CO_2 at sub-atmospheric pressures has been evaluated in a fundamental study of the equilibrium of adsorption of CO_2, N_2, H_2 and CH_4. A preliminary CO_2 uptake screening test has been carried out to discard the samples with less than 2 mol$\cdot$ kg^{-1} of CO_2 adsorbed at atmospheric pressure. Adsorption models are very useful as they can predict the behaviour of the equilibrium of adsorption over a wide range of temperatures and pressures. In order to predict multicomponent adsorption from binary CO_2-CH_4, CO_2-H_2, and CO_2-N_2 mixtures, the extended multicomponent Sips equation and the Ideal Adsorbed Solution Theory (IAST) in conjunction with the Sips model have been used and the results have been compared. Both equations deliver different conclusions regarding the heterogeneity of the adsorbate-adsorbent system. Additionally, a commercial activated carbon (Calgon BPL) was evaluated under the same operating conditions as a reference carbon adsorbent.

2. Materials and Method

Porous carbons can be prepared from a wide range of carbon-containing materials including coal, lignin, wood, peat and synthetic and natural polymers. Carbonisation and activation of these

materials under appropriate conditions yield carbons with a rather uniform pore structure consisting of micropores whose size is similar to that of the adsorbed molecules. For instance, low-density materials can be prepared by carbonisation of polymeric compounds pretreated by various procedures, including modification with inorganic additives [15]. In particular, carbon sorbents with exactly the prescribed structure have been prepared using NaCl [16] and silicon [17] additives.

2.1. Synthesis of Carbon Precursors

Phenol-formaldehyde (PF) resins were used in this work to produce carbon-based microporous materials. Synthesis was conducted following two different routes, acid (hydrochloric acid, 37 wt% HCl solution) and basic (sodium hydroxide, NaOH) catalysis for the Novolac and the Resol resins, respectively. Details on the synthesis of the PF resins can be found elsewhere [18]. Carbon precursors were prepared from the aforementioned resins, and potassium chloride (KCl) was incorporated as inorganic additive. One set of materials was impregnated with a saturated KCl solution at ambient temperature (set *a*) while another was boiled in a saturated KCl solution (set *b*). Another carbon precursor was prepared by mixing PF resin with an agricultural by-product, olive stones (OS), at a proportion of 20:80 wt% of PF to OS. A curing agent, hexamethylenetetramine (hexa) was added to PF at a hexa ratio of 7:2 wt%. Table 1 summarizes the materials and conditions for the production of the PF resin-derived carbon precursors.

Table 1. Departing materials and conditions for the production of PF resin-derived carbon precursors.

Precursor	Type of PF Resin	F/P *	Curing (Tmax, °C)	Additive Incorporation	K/R **
ReKCla	Basic catalysis (Re)	2.5:1	80	Ambient KCl	1.7
ReKClb	Basic catalysis (Re)	2.5:1	80	Boiling KCl	1.9
No1KCla	Acid catalysis (No1)	1:1.2	100	Ambient KCl	2.1
No1KClb	Acid catalysis (No1)	1:1.2	100	Boiling KCl	1.7
No2OS	Acid catalysis (No2)	1:1	170	OS (20:80) and hexa (7:2)	—

* F/P: formaldehyde to phenol molar ratio; ** K/R: potassium chloride to resin weight ratio.

2.2. Production of Microporous Carbons

The prepared carbon precursors were first carbonised and then activated with CO_2 to develop their microporous structure, preferably in the narrow microporosity domain (pore sizes of less than 1 nm) since CO_2 adsorption at sub-atmospheric pressures is known to focus on the narrow micropores [15,19,20].

Carbonisation was conducted in a tubular furnace under an inert atmosphere (50 mL· min^{-1} of N_2). Two different temperature programs were selected for PF-KCl; the two precursors of set *a* were subjected to a one-step carbonisation procedure at 600 °C for 1.5 h while for set *b*, a three-step slow carbonisation treatment at 200 (1 h), 600 (0.5 h) and 1000 °C (0.5 h) was carried out. The PF-OS composite was carbonised at 1000 °C (0.2 h) by slowly heating from ambient temperature at 4 °C· min^{-1}.

Activation with carbon dioxide favours the development of microporosity [21]. The largest increase in porosity is produced in the early stages of the activation process. Burn off (*i.e.*, degree of activation) increases the widening of existing micropores but external burning of the particle outweighs the creation of new porosity, resulting in a net destruction of porosity, especially above 40%–50% burn off [22]. Control of the activation parameters (temperature and burn off degree) is crucial for tailoring the micropore size distribution. Previous works carried out in our research group have demonstrated the relationship between the volume of narrow micropores of less than 0.7 nm and CO_2 uptake at atmospheric pressure [20]. Response surface methodology was performed to obtain the optimum conditions of activation with CO_2 that maximise CO_2 adsorption at atmospheric pressure for each precursor (details can be found in [18]). Activation with CO_2 was conducted in a tubular furnace with a CO_2 flowrate of 10 mL· min^{-1}. Table 2 summarises the conditions of the carbonisation and

activation with CO_2 steps. Yields of char production during carbonisation were around 40% for PF-KCl precursors independently of the carbonisation temperature selected or type of PF resin (acid, No, or basic, Re), and slightly lower for PF-OS due to the high volatile matter content of the biomass: olive stones. Higher activation temperatures were required for the No1KCl than for the ReKCl precursors and even higher ones for No2OS. The burn off degrees ranged between 10 and 50%, the two limits of the experimental region tested, for the ReKCl precursors while intermediate values were found to be optimal for the No1KCl and No2OS precursors. It should be noted that for precursors No1KClb and No2OS the burn off was not statistically significant, according to the response surface methodology. Consequently, the lowest burn off to yield the highest experimental CO_2 uptake was selected. For the sense of clarity and simplicity the activated samples will be denoted hereafter as follows: RKa-A71 (ReKCla activated carbon), RKb-A75 (ReKClb activated carbon), NKa-A82 (No1KCla activated carbon), NKb-A82 (No1KClb activated carbon) and NOS-A94 (No2OS activated carbon).

Table 2. Conditions of carbonisation and activation with CO_2 for each precursor.

Activated Material	Precursor	Carbonisation		Activation	
		Temp. (°C)	Yield (%) *	Temp. (°C)	Burn off (%) **
RKa-A71	ReKCla	600	40	694	10
RKb-A75	ReKClb	1000	39	722	50
NKa-A82	No1KCla	600	37	810	22
NKb-A82	No1KClb	1000	40	800	20
NOS-A94	No2OS	1000	32	940	38

* Char yield has been estimated as *yield* (%) = $(m_c/m_i) \times 100$, where m_c is the mass of char produced and m_i is the mass of raw precursor; ** Burn off or degree of activation is estimated as *burn off* (%) = $(m_c - m_a) \times 100/m_c$, where m_c is the mass of char and m_a is the mass of activated sample produced.

3. Results and Discussion

3.1. Chemical and Textural Characterisation

The elemental composition (carbon, hydrogen and oxygen contents) of the PF resins, the PF-KCl and PF-OS precursors and the corresponding chars and activated materials were determined using a LECO CHN-2000 analyzer. The acid/basic character of the carbon surfaces was evaluated by means of the Point of Zero Charge (pH_{PZC}), as determined by mass titration. The data are presented in Table 3.

Table 3. Chemical characteristics of the materials.

Sample	Elemental Composition (wt%, daf)			pH_{PZC}
	C	H	O *	
Resol-based series				
Re	74.7	5.9	19.4	7.2
ReKCla char	94.7	2.2	3.1	8.5
RKa-A71	96.2	1.3	2.5	9.5
ReKClb char	91.0	0.8	8.2	9.4
RKb-A75	92.7	1.1	6.2	9.6
Novolac-based series				
No1	82.6	6.0	11.4	5.2
No1KCla char	96.5	0.5	3.0	4.6
NKa-A82	99.0	0.4	0.6	8.7
No1KClb char	97.0	0.4	2.6	7.6
NKb-A82	99.0	0.6	0.4	8.5
No2	78.1	5.8	16.1	4.8
No2OS char	96.3	0.8	2.9	7.4
NOS-A94	98.0	0.4	1.6	8.4

daf: dry ash free basis; * calculated by difference.

The synthesised resins, Re, No1 and No2, do not contain nitrogen and so it has not been included in the table. As expected for a carbon precursor the C contents in the initial resins are high (>70 wt%) and are enhanced during the subsequent steps of carbonisation and activation. The resultant activated materials present C contents well above 90 wt% at the expense of a reduction in the volatile matter content, here represented by the O and H contents.

There is a basification effect on the carbon surfaces as a consequence of the activation with CO_2. This effect is particularly significant in the case of the activated carbons produced from the acid catalyzed resins (No1 and No2). Basicity might be ascribed to basic oxygen functionalities incorporated from the activating gas (CO_2) or to Lewis type basic sites associated to the carbon structure [11].

Textural characterisation of the samples mainly involved the evaluation of the microporosity (pore sizes < 2 nm), given the critical role of these pore sizes on the CO_2 adsorption capacity of the samples. The N_2 and CO_2 adsorption isotherms at −196 and 0 °C, respectively (Figure 1a,b), were determined in a Micromeritics TriStar 3000 volumetric apparatus. Prior to any measurements, the samples were outgassed overnight at 100 °C under vacuum.

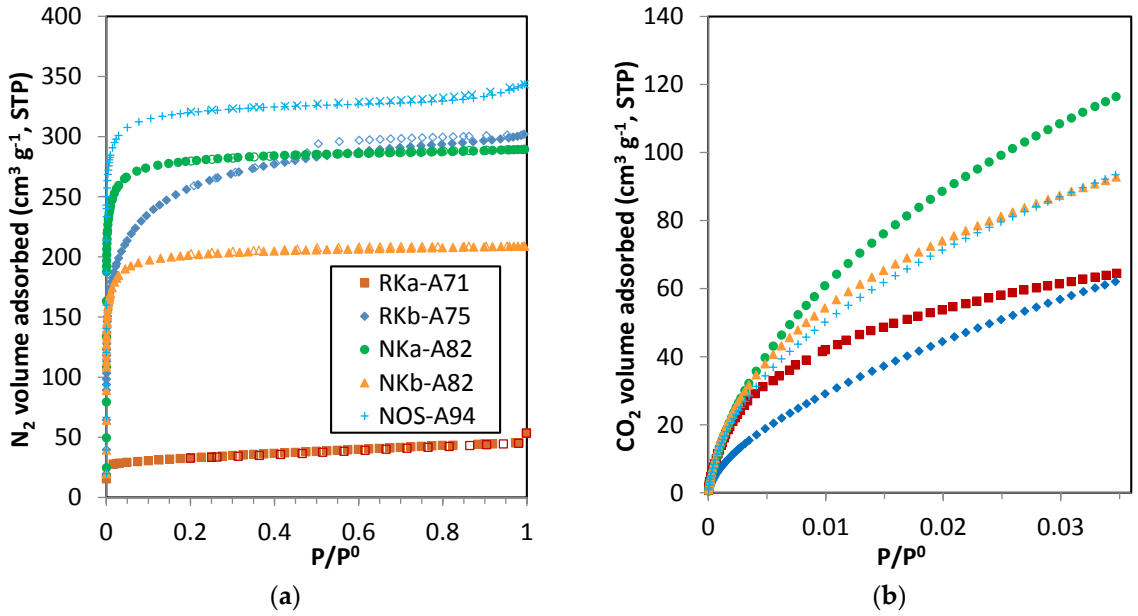

Figure 1. N_2 adsorption isotherms at −196 °C (**a**) and CO_2 adsorption isotherms at 0 °C (**b**) for the activated carbons tested (bold symbols represent adsorption and empty symbols desorption).

The five tested activated carbons exhibited distinctive textural features, as can be observed in Figure 1a. RKa-A71 is the least developed in terms of total porosity but shows a type I isotherm, according to the IUPAC classification, characteristic of strictly microporous materials. RKb-A75 presents a wider microporosity, characterised by a more open knee at low relative pressures, and it also shows a hysteresis loop at relative pressures above 0.4, which suggests the presence of some mesoporosity in the sample. On the other hand, NKa-A82 and NKb-A82 display similar type I isotherms but with different volumes of adsorbed N_2 along the evaluated pressures. NOS-A94 is the sample that has the most extended textural development, particularly in the domain of microporosity. Regarding CO_2 adsorption at 0 °C (Figure 1b), the uptake of the activated carbons follows the order: NKa > NKb ≈ NOS > RKa > RKb. RKa-A71 is the sample with the narrowest microporosity as reflected by the more pronounced curvature of the CO_2 isotherm.

The micropore volumes (W_0) and average micropore widths (L_0) were determined by applying the Dubinin–Radushkevich (DR) relation [23] and the Stoeckli-Ballerini relation [24] to these isotherms, respectively. This allowed the total microporosity and the narrow microporosity (pore sizes <1 nm)

to be assessed. The textural parameters estimated from the experimental N_2 and CO_2 isotherms are collected in Table 4.

Table 4. Textural parameters evaluated from the N_2 and CO_2 adsorption isotherms at −196 and 0 °C, respectively.

Parameter	RKa-A71	RKb-A75	NKa-A82	NKb-A82	NOS-A94
V_p ($cm^3 \cdot g^{-1}$)	0.08	0.46	0.45	0.32	0.53
$W_{0,N2}$ ($cm^3 \cdot g^{-1}$)	-	0.35	0.44	0.32	0.50
$L_{0,N2}$ (nm)	-	1.80	1.00	1.23	0.82
$W_{0,CO2}$ ($cm^3 \cdot g^{-1}$)	0.21	0.18	0.38	0.31	0.27
$L_{0,CO2}$ (nm)	0.58	0.70	0.71	0.64	0.64

As expected, in agreement with the shape of the corresponding isotherms, most of the porosity in NKa-A82, NKb-A82 and NOS-A94 lies in the microporosity domain. To be more precise, NKb-A82 concentrates its microporosity in the narrow microporosity range, whereas NKa-A82 and, particularly, NOS-A94 have a wider microporosity. Samples RKa-A71 and RKb-A75 show similar narrow micropore volumes ($W_{0,CO2}$). The textural development of RKa-A71 is restricted to this narrow microporosity, whereas RKb-A75 also presents supermicropores (1–2 nm) and mesopores (2–50 nm) as can be inferred from the differences between V_p, $W_{0,N2}$ and $W_{0,CO2}$. Average micropore widths ($L_{0,N2}$) of around 1 nm for the NK and NOS based ACs and *ca.* 2 nm for the RKb-A75 sample were assessed. The narrow microporosity ($L_{0,CO2}$) fell within the 0.6–0.7 nm range. The route selected to synthesise the PF precursor compromised the textural development that could have been achieved for the activated carbon. In order to gain a better insight into the narrow microporosity, the pore size distributions in the range of 0.3–1 nm were estimated by means of the Density Functional Theory (DFT) for CO_2 adsorption onto slit pore carbons using Micromeritics' software (method: non-negative regularization, little smoothing). The plots are shown in Figure 2.

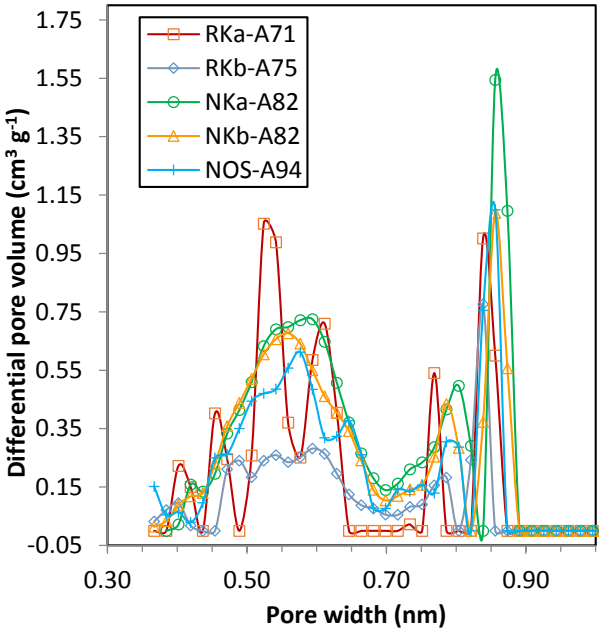

Figure 2. Micropore size distributions from the CO_2 adsorption isotherms at 0 °C by means of the DFT slit pore carbon model.

The narrow micropore size distributions of the studied materials can be described as bimodal as they present two main peaks with characteristic pore sizes in the range of 0.55–0.65 and 0.8–0.9 nm,

respectively. The bimodal shape of the pore size distributions is a characteristic feature for many adsorbents possessing even a small amount of micropores. It is shown that this feature results from the similarity of the local adsorption isotherm in the range of the pore widths for which the gap between peaks (related to the primary and secondary micropore filling mechanism) exists [25].

Generally, the tested carbons show striking similarities in the pore size distributions. Sample RKa-A71 seems the exception as it shows a narrower micropore size distribution. The sizes of the narrow micropores in the materials are highly suitable for the separation of CO_2 at sub-atmospheric pressures [15,20].

3.2. CO_2 Uptake Screening

The CO_2 adsorption capacity of the produced carbons was first evaluated at sub-atmospheric pressures and room temperature. CO_2 adsorption isotherms at 25 °C and up to 101 kPa were determined in a Quantachrome Nova 4000 volumetric device. The samples were previously outgassed overnight at 100 °C under vacuum. A commercial activated carbon, Calgon BPL, was also tested for reference purposes [26]. This is a Calgon Carbon granular activated carbon specifically designed for use in gas phase applications. The measured isotherms are plotted in Figure 3.

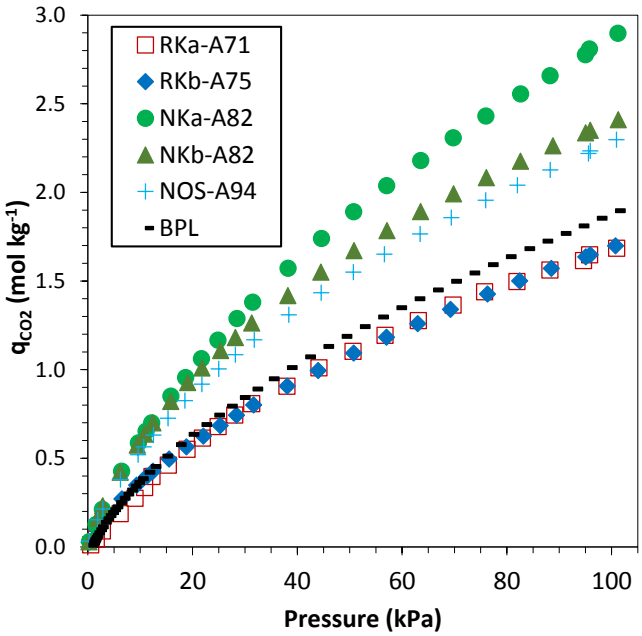

Figure 3. CO_2 adsorption isotherms at 25 °C and sub-atmospheric pressures for the studied carbons.

The NK and NOS carbons showed substantial CO_2 uptakes over the sub-atmospheric pressure range tested, with isotherms characterised by more pronounced slopes at pressures below 20 kPa. Maximum CO_2 uptakes of 2.9, 2.4 and 2.3 mol· kg^{-1} were achieved at 101 kPa for samples NKa-A82, NKb-A82 and NOS-A94, respectively. The isotherms of the two NK samples nearly overlapped in the pressure range below 20 kPa, as might be expected from the similarities in the narrower microporosity of both samples. When the pressure approaches the atmospheric value, differences in the CO_2 adsorption capacity appeared revealing the different microporosity features of the two NK activated carbons. The performance of carbon NOS shows striking similarities to that of NKb in agreement with the similarities in the narrow microporosity of both samples. The RK carbons showed similar performances to that of the commercial activated carbon over the tested pressure range with maximum CO_2 uptakes of less than 2 mol· kg^{-1} at 101 kPa. Taking 2 mol· kg^{-1} as the screening value for selecting optimum CO_2 adsorbents, RK carbons were discarded for further study.

3.3. Binary Adsorption from Mixtures of CO_2-H_2, CO_2-CH_4, and CO_2-N_2

3.3.1. Single-Component Adsorption Isotherms

H_2, CH_4, and N_2 adsorption isotherms at 25 °C and sub-atmospheric pressures (up to 100.3 kPa) for the NK and NOS carbons were obtained using a Micromeritics TriStar 3000 volumetric equipment. BPL was also tested for comparison purposes. Detailed textural characteristics of this activated carbon can be found elsewhere [27]. Prior to analysis the samples were outgassed overnight at 100 °C under vacuum.

Experimental data of the single component CO_2, H_2, CH_4, and N_2 adsorption isotherms were fitted to the Sips equation, as follows:

$$\text{Sips equation: } q = q_s \frac{(bP)^{1/n}}{1 + (bP)^{1/n}} \quad (1)$$

where q represents the concentration of the adsorbed species, q_s the saturation capacity and P the pressure of the adsorptive. The parameters b, n and q_s are temperature dependent; b usually takes the form of the adsorption affinity. The parameter n shows the heterogeneity of the system and its value is usually greater than unity; therefore, the larger the value of n, the more heterogeneous the system is.

This empirical three-parameter equation has been widely used for fitting the isotherm data of different hydrocarbons on activated carbon. The Sips equation is believed to give a more accurate fit over a larger pressure regime than the standard Langmuir or Freundlich equations, and provides more accurate prediction of the quantity adsorbed at saturation than the Langmuir equation for heterogeneous adsorbents. However, it suffers from the same disadvantage as the Freundlich equation: it does not reduce to Henry's Law at low surface coverage [28].

Fitting of the model to the experimental data was conducted by means of the *Solver* Excel tool (Microsoft Office Excel 2010) departing from values of q_s and n of 1 and b of 0. The goodness of the fit was evaluated on the basis of the minimum squared relative error (SRE) as given by the following expression:

$$SRE(\%) = \sqrt{\frac{\sum_i \left[\left(q_{\text{exp},i} - q_{\text{mod},i}\right)/q_{\text{exp},i}\right]^2}{N-1}} \times 100 \quad (2)$$

where $q_{exp,i}$ and $q_{mod,i}$ are the experimental and Sips-predicted adsorbed amounts of component i, respectively, and N is the number of experimental data points. The optimal parameters and squared relative errors from fitting the Sips model to the single-component data of CO_2, H_2, CH_4, and N_2 at 25 °C are summarized in Table 5. Isotherm experimental data and fittings to the Sips model are shown in Figure 4.

The experimental adsorption data show that much more CO_2 is adsorbed than CH_4 and more significantly than N_2 and H_2 on the tested carbons. The differences in CO_2, CH_4 and N_2 uptake may be explained by the larger quadrupole moment of CO_2 that produces a strong attraction towards the adsorbent surface resulting in a greater uptake. The high level of polarizability of CO_2 and CH_4 can create a momentary shift in its neutral electrostatic field but this attraction force is much weaker than the quadrupole moment [29]. In contrast, N_2 molecules are nonpolar and smaller, compared with CH_4 molecules. For this reason, the differences in CO_2 and N_2 uptake are greater than the differences in CO_2 and CH_4 uptake. Since the narrow micropores allow the strongest interaction between the carbonaceous solid and the hydrogen molecule, it is to be expected that this fraction of the porous volume will make a major contribution to the hydrogen adsorption capacity of the materials. Although hydrogen should only interact through induced polarization, surface chemistry may influence hydrogen adsorption on carbonaceous surfaces, particularly at sub-atmospheric pressures [30,31].

Table 5. Optimal parameters of the single-component CO_2, CH_4, H_2, and N_2 adsorption data fitting to the Sips model.

Sample	CO_2			*SRE* (%)	CH_4			*SRE* (%)
	q_s	b	n		q_s	b	n	
NKa-A82	7.37	5.77×10^{-3}	1.17	1.1	3.76	5.69×10^{-3}	1.10	1.5
NKb-A82	5.38	7.46×10^{-3}	1.24	1.0	3.37	3.13×10^{-3}	1.15	1.9
NOS-A94	6.29	4.77×10^{-3}	1.28	0.6	4.20	2.62×10^{-3}	1.30	3.3
BPL	4.72	6.02×10^{-3}	1.17	3.0	2.63	4.03×10^{-3}	1.07	2.6
Sample	**H_2**			***SRE* (%)**	**N_2**			***SRE* (%)**
	q_s	b	n		q_s	b	n	
NKa-A82	0.39	1.50×10^{-3}	1.00	8.8	2.18	2.55×10^{-3}	1.00	1.7
NKb-A82	2.46	1.29×10^{-4}	1.00	8.2	2.87	1.17×10^{-3}	1.00	2.1
NOS-A94	1.44	4.06×10^{-5}	1.65	11.0	2.36	1.81×10^{-3}	1.00	2.1
BPL	0.41	1.98×10^{-4}	1.19	5.1	2.90	9.89×10^{-4}	1.00	2.0

q_s: mol·kg^{-1}, b: kPa^{-1}.

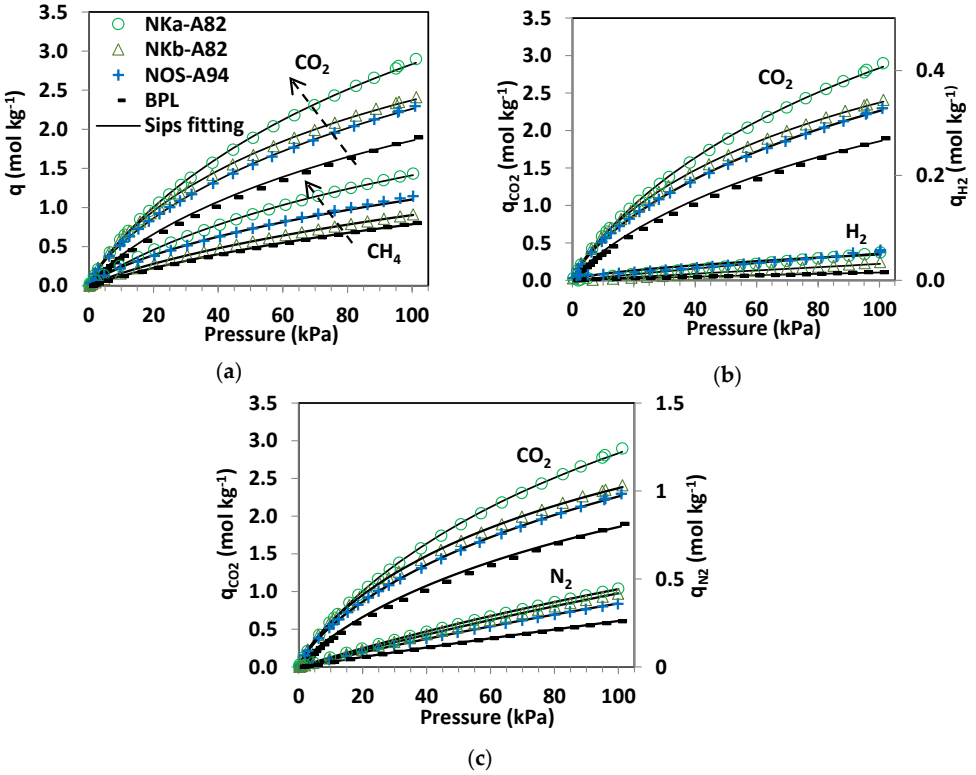

Figure 4. CO_2, CH_4 (**a**); H_2 (**b**) and N_2 (**c**) adsorption isotherms at 25 °C on samples NKa-A82, NKb-A82, NOS-A94 and BPL. Fitting of the single component adsorption data to the Sips model is represented by the solid lines.

By comparing the quantities adsorbed by the phenol-formaldehyde carbons in Figure 4 it can be seen that NKa-A82 is the sample with the greatest CO_2, CH_4, N_2 and H_2 uptakes over the sub-atmospheric pressure range tested. Moreover, the adsorption capacities of the three PF carbons are greater than that of the reference carbon, BPL. In terms of CO_2 adsorption, the performance at pressures below 20 kPa is quite similar for the NK and NOS carbons and it is only at higher pressures where NKa-A82 stands out. CH_4 adsorption isotherms show differentiated uptakes for the three PF carbons that follow the order NKa > NOS > NKb. All three samples present relevant microporosity; in sample NKb narrow micropores (<1 nm) are mainly encountered, whereas for NKa and NOS microporosity >1 nm is also present, in agreement with the textural parameters estimated from the DR

relation (see Table 4). In this scenario selectivity effects related to the kinetic diameters of the two gas molecules (3.30 Å for CO_2 and 3.80 Å for CH_4) [29] may play a role in the change in the CO_2 and CH_4 adsorption trends of the three PF carbons. N_2 and H_2 adsorption is characterised by linear isotherms that reveal the unspecific nature of the adsorbate-adsorbent interaction [32].

The pure component CO_2, H_2, CH_4, and N_2 adsorption isotherms fitted to the Sips model (Equation (1)) are represented by the continuous lines in Figure 4. The saturation capacities (q_s) and the parameter n have been fitted to the adsorption data for the four gas species independently (Table 5).

The Sips model reproduces the adsorption of CO_2, CH_4, and N_2 with good accuracy, with substantial deviations for the adsorption of H_2. It should be noted that the experimental H_2 adsorption data at sub-atmospheric pressures and ambient temperature are subject to greater uncertainty due to the significantly lower uptakes of H_2 under these conditions. The values of q_s and b follow the trend $CO_2 > CH_4 > N_2 >> H_2$, as might be expected from the experimental data where the capacity and, consequently, the affinity of the carbons to adsorb CO_2 and CH_4 is one and two orders of magnitude greater than that of N_2 and H_2, respectively. The parameter n takes values close to unity for CO_2 and CH_4 while for N_2 takes values of unity, suggesting that heterogeneity plays a minor role in these systems. The uneven fitting of the H_2 isotherms for the studied carbons can be mainly ascribed to uncertainty of the experimental data. Sample NOS is where greatest deviation from unity in the values of n is found for the adsorption of CO_2, CH_4 and H_2.

3.3.2. Multicomponent Adsorption Prediction

In order to predict multicomponent adsorption from binary CO_2-H_2, CO_2-CH_4, and CO_2-N_2 mixtures, the fitting of the single component adsorption data to the Sips model represented by Equation (1) was rerun to account for the interaction between components in each binary mixture. Given that CO_2 is the strongest adsorbate, the fitting was conducted keeping q_s constant (the value of q_s estimated from the fitting of single component CO_2 adsorption isotherm for each sample) and adjusting the b and n values to minimize the relative error for the pairs CO_2-H_2, CO_2-CH_4, and CO_2-N_2, respectively. The values of the parameters estimated from these fittings are collected in Table 6.

Table 6. Optimal parameters of the single-component CO_2, H_2, CH_4, and N_2 adsorption data fitting to the Sips model for multicomponent prediction.

Sample	**CO_2-CH_4**			
	b_{CO2}	b_{CH4}	n	***SRE* (%)**
NKa-A82	5.83×10^{-3}	2.01×10^{-3}	1.16	3.0
NKb-A82	7.99×10^{-3}	1.52×10^{-3}	1.19	2.7
NOS-A94	4.43×10^{-3}	1.36×10^{-3}	1.32	2.3
BPL	6.33×10^{-3}	1.60×10^{-3}	1.14	3.7
Sample	**CO_2-H_2**			
	b_{CO2}	b_{H2}	n	***SRE* (%)**
NKa-A82	6.55×10^{-3}	4.27×10^{-5}	1.10	7.9
NKb-A82	1.03×10^{-2}	5.33×10^{-5}	1.01	15.4
NOS-A94	4.18×10^{-3}	1.69×10^{-5}	1.35	9.6
BPL	6.08×10^{-3}	1.31×10^{-5}	1.16	4.3
Sample	**CO_2-N_2**			
	b_{CO2}	b_{N2}	n	***SRE* (%)**
NKa-A82	6.93×10^{-3}	5.36×10^{-4}	1.06	6.6
NKb-A82	9.63×10^{-3}	6.98×10^{-4}	1.06	9.6
NOS-A94	6.90×10^{-3}	5.12×10^{-4}	1.05	11.9
BPL	7.00×10^{-3}	3.75×10^{-4}	1.10	10.7

b: kPa^{-1}.

The fitted parameters follow the same trend observed in the previous independent Sips fittings: the n values are close to unity and the b values follow the order $CO_2 > CH_4 > N_2 >> H_2$. When mixed the affinity, as represented by the parameter b, increases for the strong adsorbate (CO_2) when compared

to the pure component CO_2 adsorption data independent fitting. Likewise, the weaker adsorbate shows a substantial decrease in affinity particularly in the CO_2-H_2 and CO_2-N_2 systems.

In this way, use of the parameters from the fitting of pure component data pairs guarantees the thermodynamic consistency of the resulting analytical expression of the multicomponent Sips model. Using the same analogy for extending the single-component Langmuir equation to that for multicomponent adsorption, the following equation is obtained for the multicomponent Sips model [33]:

$$q_i = \frac{q_s \left(b_i y_i P\right)^{1/n}}{1 + \sum_{j=1}^{N} \left(b_j y_j P\right)^{1/n}} \tag{3}$$

where i and j stand for the components in the binary mixture, y is the mole fraction of the corresponding component in the gas phase, and N is the number of components in the gas mixture, *i.e.*, 2. However, this equation only corresponds to a specific case of surface energetic heterogeneity. For normal activated carbons in which the energy sites are highly correlated, the Ideal Adsorbed Solution Theory (IAST) should be used. Application of the IAST with the concept of hypothetical pure-component pressure results in the following equation [34]:

$$q_i = \frac{q_s b_i y_i P \left(\sum_{j=1}^{N} b_j y_j P\right)^{(1/n)-1}}{1 + \left(\sum_{j=1}^{N} b_j y_j P\right)^{1/n}} \tag{4}$$

It can be seen that Equations (3) and (4) deliver different expressions to reproduce the multicomponent Sips model on the basis of different assumptions regarding the heterogeneity of the adsorbate-adsorbent system. Nevertheless, both equations were used in the present study to predict the binary adsorption equilibrium for CO_2-H_2, CO_2-CH_4, and CO_2-N_2 systems and the results are discussed and compared. The parameter values used for such multicomponent adsorption predictions were those previously obtained from the combined fitting of the pure component adsorption data of the pairs of gases in each mixture as shown in Table 6.

The predictions of the binary gas adsorption equilibria from the multicomponent Sips model represented by Equations (3) and (4) and from the parameters included in Table 6 are depicted in Figures 5–7. Multicomponent predictions were assessed under the following temperature and pressure conditions: 25 °C and 100 kPa.

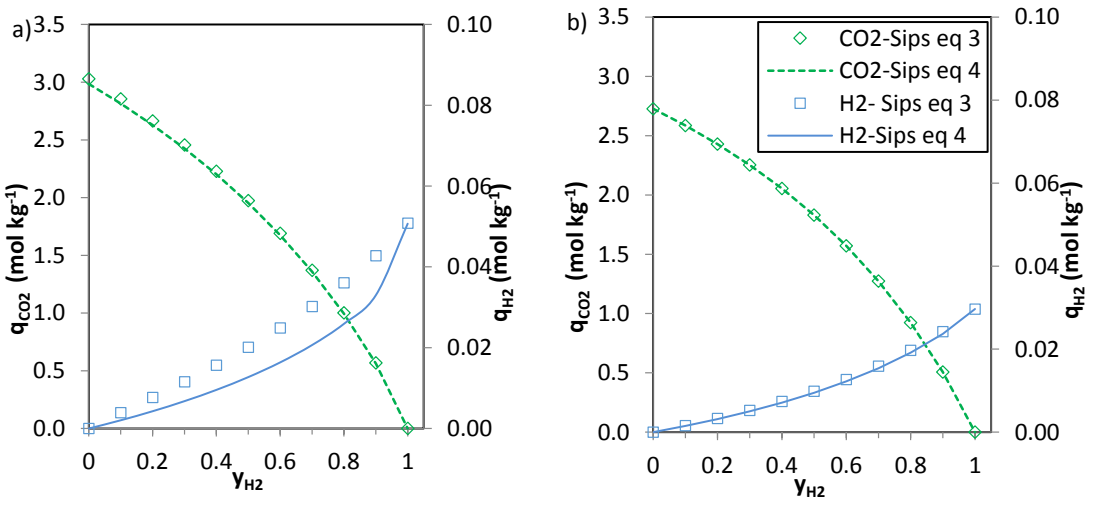

Figure 5. *Cont.*

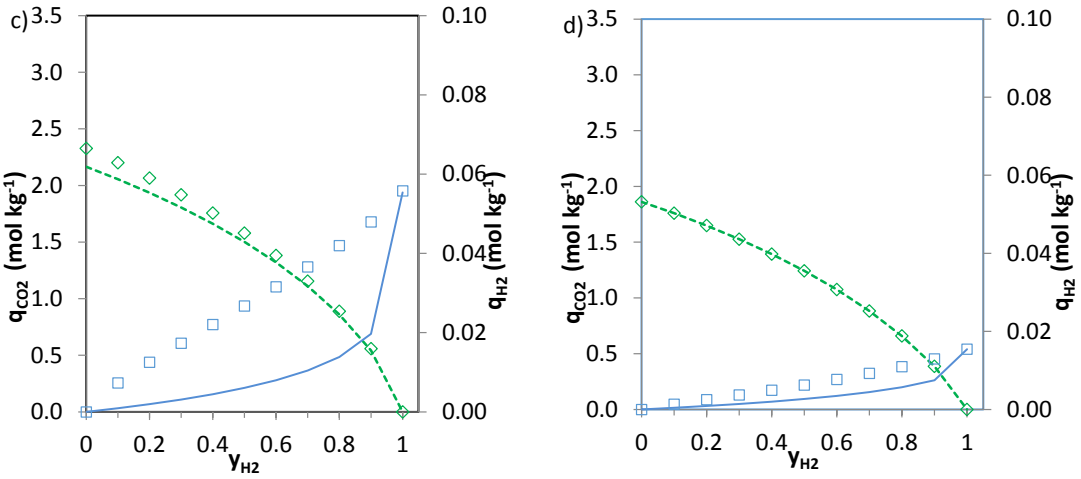

Figure 5. Multicomponent prediction by means of the Sips model for CO_2-H_2 binary mixtures at 100 kPa and 25 °C: (**a**) NKa-A82; (**b**) NKb-A82; (**c**) NOS-A94 and (**d**) BPL.

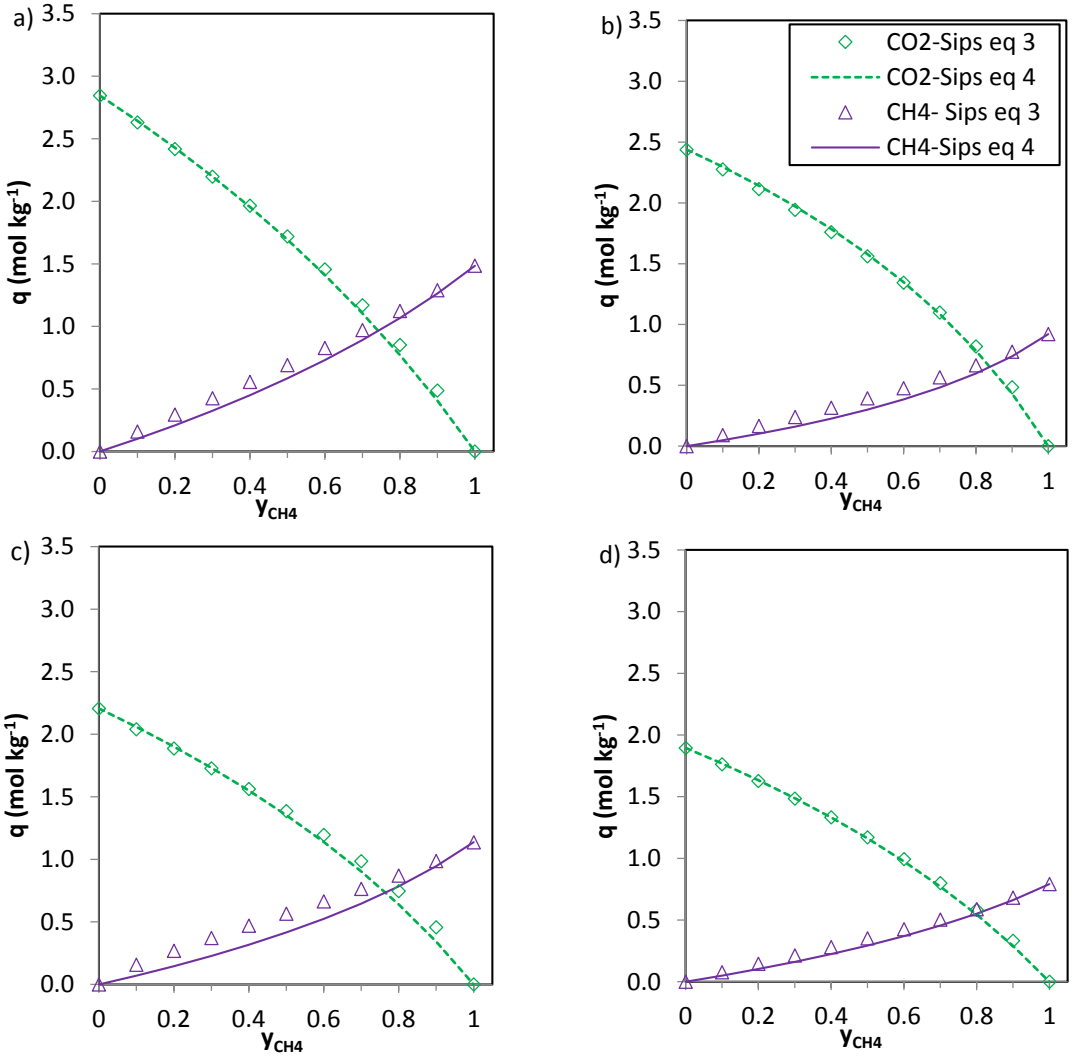

Figure 6. Multicomponent prediction by means of the Sips model for CO_2-CH_4 binary mixtures at 100 kPa and 25 °C: (**a**) NKa-A82; (**b**) NKb-A82; (**c**) NOS-A94 and (**d**) BPL.

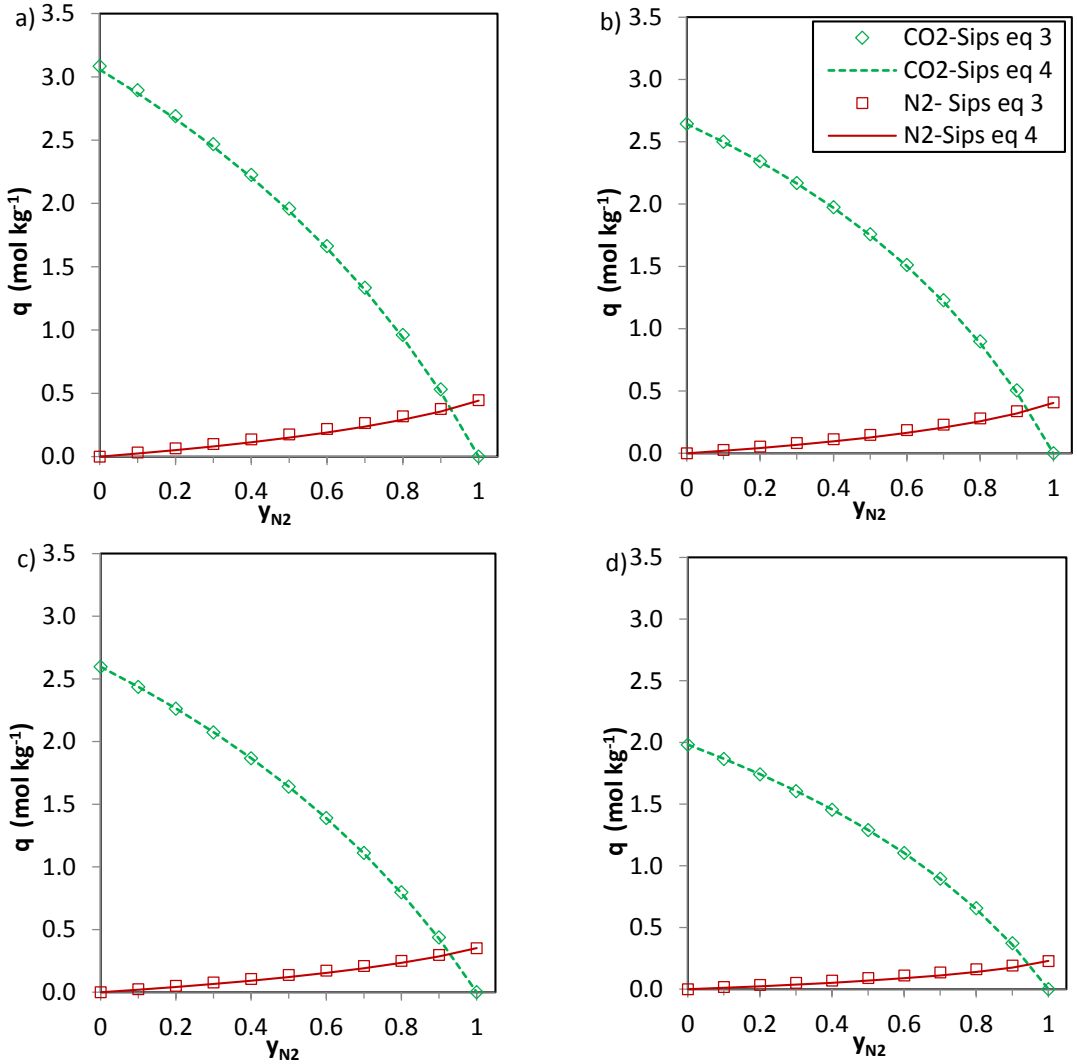

Figure 7. Multicomponent prediction by means of the Sips model for CO_2-N_2 binary mixtures at 100 kPa and 25 °C: (**a**) NKa-A82; (**b**) NKb-A82; (**c**) NOS-A94 and (**d**) BPL.

Globally, the predicted multicomponent adsorption isotherms show a reduction in the uptakes of the four components when mixed in binary CO_2-H_2, CO_2-CH_4 or CO_2-N_2 mixtures. However, while the CO_2 uptake when mixed in a 1:1 molar ratio is reduced to 60%, 70% and 75% (average values for the four evaluated carbons in the CO_2-CH_4, CO_2-N_2 and CO_2-H_2 binary mixtures, respectively) of the pure gas CO_2 adsorption at 25 °C and 100 kPa, the H_2, N_2 and CH_4 uptakes drastically drop down to around 30–35% of those corresponding to pure gas adsorption. This suggests that the presence of another component in the mixture influences the adsorption of CO_2 to a lesser extent.

It is apparent that when n (Table 6) approaches unity the values of the numerator and the denominator of Equations (3) and (4) tend to match each other and both Equations (3) and (4) give similar predictions. This suggests that there is little heterogeneity in the systems that could influence the adsorption of the binary mixtures onto the evaluated carbons. The CO_2-H_2 system is where greater deviations between the two predictions are observed, particularly for the H_2 uptake. It should be noted that at sub-atmospheric pressures and room temperature experimental H_2 adsorption is characterised by extremely low uptakes. In addition, the affinity of the carbons towards H_2 adsorption is significantly lower than that to CO_2. Consequently, binary adsorption prediction for the CO_2-H_2 system is subject to greater uncertainty. Moreover, predicted CO_2 adsorption in the CO_2-H_2 binary mixtures nearly matches pure component CO_2 adsorption at similar partial pressures suggesting that H_2 adsorption in

these mixtures can be considered as negligible. This is in agreement with previous results from the research team [6,35].

The CO_2 uptake at $y_j = 0$ (where j stands for H_2, N_2 and CH_4, respectively) is slightly overestimated for the CO_2-H_2 and CO_2-N_2 systems compared to the pure component CO_2 adsorption data. This may be attributed to the different affinity of the adsorbent towards CO_2 and H_2 or N_2.

In the case of CO_2-CH_4 (Figure 6) and CO_2-N_2 (Figure 7) the predictions of the two Equations (3) and (4) seem consistent. The values of n (Table 6) are close to unity for the CO_2-N_2 system and thus Equations 3 and 4 deliver similar predictions. For the phenolic resin-biomass composite derived carbon, NOS-A94, Equation (3) predicts slightly greater CH_4 uptakes (+0.15 mol·kg^{-1}) than Equation (4) for molar fractions of methane (y_{CH4}) in the binary mixture between 0.3 and 0.6. Both CO_2 and CH_4 show specific interaction with the carbon surface, as reflected by the shape of the isotherms (type I, according to the IUPAC classification). However, despite the preferential adsorption of CO_2 over CH_4, competition between both adsorbates exists. The significantly higher critical temperature of CO_2 in comparison with CH_4 makes carbon dioxide more likely to behave as a condensable steam than as a supercritical gas, making it less volatile and increasing its chances of adsorption. Moreover, CO_2 presents a higher polarizability which may enhance attractive forces with the surface and a permanent quadrupole, leading to stronger interactions with any solid surface.

The simplified extended Sips model (Equation (3)) shows limitations bearing in mind the assumptions needed to extend the single component Sips equation to the multicomponent one. However, the observed deviations between the multicomponent predictions represented by Equations (3) and (4) are small and therefore, both could be applied to predict the adsorption of CO_2, CH_4, and N_2 on the evaluated carbons in binary CO_2-CH_4, and CO_2-N_2 mixtures. The H_2 uptakes predicted for the CO_2-H_2 systems should be handled with care given the uncertainty of the experimental H_2 adsorption data under sub-atmospheric pressures and room temperature. H_2 adsorption can be regarded as negligible in the CO_2-H_2 systems. Moreover, data on the performance of the phenolic resin-derived carbon for CO_2-CH_4 adsorption were also experimentally obtained in a lab scale fixed-bed adsorption unit. Details can be found elsewhere [6]. The CO_2 and CH_4 uptakes assessed at 120 kPa and 25 °C for a 1:1 CO_2:CH_4 binary mixture are in good agreement with the multicomponent predictions at 100 kPa and 25 °C presented herein; for instance, the predicted CO_2 uptake on carbon NKa-A82 for a 1:1 CO_2:CH_4 mixture at 120 kPa is 1.90 mol·kg^{-1} in agreement with 2.03 mol·kg^{-1} estimated experimentally.

3.4. Selectivity to CO_2 Separation

The selectivity of the prepared carbons to separate CO_2 from CO_2-H_2, CO_2-N_2 and CO_2-CH_4 mixtures at ambient temperature and sub-atmospheric pressures was evaluated on the basis of the multicomponent adsorption predictions. The following expression was used:

$$S_{1/2} = \frac{q_1/q_2}{y_1/y_2} \tag{5}$$

where q_1 stands for the CO_2 uptake of the carbon from the binary mixture and q_2 represents the H_2, N_2 and CH_4 uptakes, respectively. y_1 and y_2 are the corresponding molar fractions of the gas component in the binary mixtures. From the IAST-Sips multicomponent adsorption model represented by Equation (4), the following equation can be inferred to account for the selectivity to separate CO_2 from binary mixtures:

$$S_{1/2} = \frac{b_1}{b_2} \tag{6}$$

where b_1 and b_2 stand for the affinity constants of CO_2 and H_2, N_2 and CH_4, respectively. According to Equation (6) the selectivity to separate CO_2 from binary mixtures is independent of the partial pressures of the components in the binary mixture. Table 7 summarizes the selectivities of the carbons as estimated from Equation (6) (b_1:b_{CO2} and b_2:b_{H2}, b_{N2} *or* b_{CH4}).

Table 7. Selectivities of the carbons to separate CO_2 from CO_2-H_2, CO_2-N_2 and CO_2-CH_4 binary mixtures.

$S_{1/2}$	CO_2-H_2	CO_2-N_2	CO_2-CH_4
NKa-A82	153	12.9	2.9
NKb-A82	193	13.8	5.3
NOS-A94	247	13.5	3.3
BPL	464	18.7	3.9

The selectivity values follow the order CO_2-H_2 >> CO_2-N_2 > CO_2-CH_4 indicating that the separation of CO_2 from CO_2-H_2 mixtures at sub-atmospheric pressures and ambient temperature is favoured. BPL shows the greatest selectivity values to separate CO_2 from CO_2-H_2 and CO_2-N_2 binary mixtures whereas the phenolic resin-derived carbon NKb-A82 presents the highest selectivity for CO_2 to be separated from CO_2-CH_4 mixtures. Nevertheless, selectivity values for the four evaluated carbons are in the same order of magnitude for each mixture and the values are particularly close in the case of CO_2-N_2 and CO_2-CH_4 separation.

The selectivity value, as estimated from Equation (6), could serve as a rough sorbent selection parameter. However, for a more precise evaluation the working capacities (differences between the gas uptakes of both components under adsorption and regeneration conditions) and the heat required for the regeneration of the adsorbent would also need to be taken into account [36].

4. Conclusions

Phenolic resin-derived carbons were prepared and evaluated for CO_2 adsorption at sub-atmospheric pressures. Single component adsorption isotherms of CO_2, H_2, N_2 and CH_4 were measured at 25 °C and up to 100 kPa and fitted to the Sips model. Binary adsorption from CO_2-H_2, CO_2-N_2 and CO_2-CH_4 mixtures was then predicted by applying the extended multicomponent Sips model and the Ideal Adsorbed Solution Theory (IAST) in conjunction with the Sips model. Both equations showed similar predictions for the adsorption of CO_2, CH_4 and N_2 on the evaluated carbons in the binary mixtures. The adsorption of H_2 at the conditions evaluated can be considered negligible. Both Sips multicomponent equations might predict binary adsorption in the studied systems. This is a significant advantage from the viewpoint of computational modelling requirements in adsorption process design.

In terms of CO_2 uptake, the performance of the acid resin-derived carbons in separating CO_2 from CO_2-CH_4, CO_2-H_2, and CO_2-N_2 at atmospheric pressure was superior to that of a reference commercial carbon (Calgon BPL) and an even higher selectivity towards CO_2 was found in the separation of CO_2-CH_4.

Acknowledgments: This work was carried out with financial support from the Spanish MINECO (Project ENE2011-23467), and was co-financed by the European Regional Development Fund (ERDF) and the Gobierno del Principado de Asturias (PCTI-GRUPIN14-079). N.A-G. acknowledges a fellowship awarded by the Spanish MINECO (FPI program), and co-financed by the European Social Fund.

Author Contributions: N.A.-G. and M.M conducted experimental work. N.A.-G. and C.P. carried out data analysis and calculations. N.A.-G., M.V.G., F.R. and C.P. discussed the results and contributed to the writing of the manuscript.

Conflicts of Interest: Authors declare no conflicts of interest.

References

1. Dovì, V.G.; Friedler, F.; Huisingh, D.; Klemeš, J.J. Cleaner energy for sustainable future. *J. Clean. Prod.* **2009**, *17*, 889–895. [CrossRef]
2. Chen, W.-H.; Chen, S.-Y.; Kumar Khanal, S.; Sung, S. Kinetic study of biological hydrogen production by anaerobic fermentation. *Int. J. Hydrog. Energy* **2006**, *31*, 2170–2178. [CrossRef]

3. Redwood, M.; Paterson-Beedle, M.; Macaskie, L. Integrating dark and light bio-hydrogen production strategies: Towards the hydrogen economy. *Rev. Environ. Sci. Biotechnol.* **2009**, *8*, 149–185. [CrossRef]
4. Gómez, X.; Fernández, C.; Fierro, J.; Sánchez, M.E.; Escapa, A.; Morán, A. Hydrogen production: Two stage processes for waste degradation. *Bioresour. Technol.* **2011**, *102*, 8621–8627. [CrossRef] [PubMed]
5. Lee, Y.-W.; Chung, J. Bioproduction of hydrogen from food waste by pilot-scale combined hydrogen/methane fermentation. *Int. J. Hydrog. Energy* **2010**, *35*, 11746–11755. [CrossRef]
6. Gil, M.V.; Álvarez-Gutiérrez, N.; Martínez, M.; Rubiera, F.; Pevida, C.; Morán, A. Carbon adsorbents for CO_2 capture from bio-hydrogen and biogas streams: Breakthrough adsorption study. *Chem. Eng. J.* **2015**, *269*, 148–158. [CrossRef]
7. Redondas, V.; Gómez, X.; García, S.; Pevida, C.; Rubiera, F.; Morán, A.; Pis, J.J. Hydrogen production from food wastes and gas post-treatment by CO_2 adsorption. *Waste Manag.* **2012**, *32*, 60–66. [CrossRef] [PubMed]
8. González, A.S.; Plaza, M.G.; Rubiera, F.; Pevida, C. Sustainable biomass-based carbon adsorbents for post-combustion CO_2 capture. *Chem. Eng. J.* **2013**, *230*, 456–465. [CrossRef]
9. Marsh, H.; Rodríguez-Reinoso, F. *Activated Carbon*; Elsevier Science Ltd.: Oxford, UK, 2006; p. 529.
10. Foley, H.C. Carbogenic molecular sieves: Synthesis, properties and applications. *Microporous Mater.* **1995**, *4*, 407–433. [CrossRef]
11. Martin, C.F.; Plaza, M.G.; Garcia, S.; Pis, J.J.; Rubiera, F.; Pevida, C. Microporous phenol-formaldehyde resin-based adsorbents for pre-combustion CO_2 capture. *Fuel* **2011**, *90*, 2064–2072. [CrossRef]
12. Martín, C.F.; García, S.; Beneroso, D.; Pis, J.J.; Rubiera, F.; Pevida, C. Precombustion CO_2 capture by means of phenol-formaldehyde resin-derived carbons: From equilibrium to dynamic conditions. *Sep. Purif. Technol.* **2012**, *98*, 531–538. [CrossRef]
13. Foster, A.I.; Linney, H.J.; Tennison, S.R.; Cory, R.A.; Swan, D.P. The use of carbons produced from phenolic resins for flue gas desulphurization. *Fuel* **1993**, *72*, 337–342. [CrossRef]
14. Tennison, S.R. Phenolic-resin-derived activated carbons. *Appl. Catal. A Gen.* **1998**, *173*, 289–311. [CrossRef]
15. Presser, V.; McDonough, J.; Yeon, S.-H.; Gogotsi, Y. Effect of pore size on carbon dioxide sorption by carbide derived carbon. *Energy Environ. Sci.* **2011**, *4*, 3059–3066. [CrossRef]
16. Hopper, R.W.; Pekala, R.W. Low density microcellular carbon or catalytically impregnated carbon forms and process for their preparation. Patent number US4806290, 1989.
17. Ryoo, R.; Joo, S.H.; Jun, S. Synthesis of highly ordered carbon molecular sieves via template-mediated structural transformation. *J. Phys. Chem. B* **1999**, *103*, 7743–7746. [CrossRef]
18. Gil, M.V.; Martínez, M.; García, S.; Rubiera, F.; Pis, J.J.; Pevida, C. Response surface methodology as an efficient tool for optimizing carbon adsorbents for CO_2 capture. *Fuel Process. Technol.* **2013**, *106*, 55–61. [CrossRef]
19. Vishnyakov, A.; Ravikovitch, P.I.; Neimark, A.V. Molecular level models for CO_2 sorption in nanopores. *Langmuir* **1999**, *15*, 8736–8742. [CrossRef]
20. Martín, C.F.; Plaza, M.G.; Pis, J.J.; Rubiera, F.; Pevida, C.; Centeno, T.A. On the limits of CO_2 capture capacity of carbons. *Sep. Purif. Technol.* **2010**, *74*, 225–229. [CrossRef]
21. Marsh, H.; Rodríguez-Reinoso, F. Chapter 5—Activation processes (thermal or physical). In *Activated Carbon*; Elsevier Science Ltd.: Oxford, UK, 2006; pp. 243–321.
22. Molina-Sabio, M.; González, M.T.; Rodriguez-Reinoso, F.; Sepúlveda-Escribano, A. Effect of steam and carbon dioxide activation in the micropore size distribution of activated carbon. *Carbon* **1996**, *34*, 505–509. [CrossRef]
23. Dubinin, M.M. Physical adsorption of gases and vapors in micropores. In *Progress in Surface and Membrane Science*; Academic Press: New York, NY, USA, 1975; Volume 9, pp. 1–69.
24. Stoeckli, F.; Ballerini, L. Evolution of microporosity during activation of carbon. *Fuel* **1991**, *70*, 557–559. [CrossRef]
25. Gauden, P.A.; Terzyk, A.P.; Jaroniec, M.; Kowalczyk, P. Bimodal pore size distributions for carbons: Experimental results and computational studies. *J. Colloid Interface Sci.* **2007**, *310*, 205–216. [CrossRef] [PubMed]
26. Corporation, C.C. BPL 4x10 Product Bulletin. Available online: http://www.calgoncarbon.com/media/images/site_library/370_BPL4x10_webp.pdf (accessed on 1 October 2015).
27. Frère, M.; De Weireld, G.; Jadot, R. Characterization of porous carbonaceous sorbents using high pressure CO_2 adsorption data. *J. Porous Mater.* **1998**, *5*, 275–287. [CrossRef]

28. Do, D.D. *Adsorption Analysis: Equilibria and Kinetics*; Imperial College London: London, UK, 1998.
29. Bárcia, P.S.; Bastin, L.; Hurtado, E.J.; Silva, J.A.C.; Rodrigues, A.E.; Chen, B. Single and multicomponent sorption of CO_2, CH_4 and N_2 in a microporous metal-organic framework. *Sep. Sci. Technol.* **2008**, *43*, 3494–3521. [CrossRef]
30. Gadiou, R.; Saadallah, S.-E.; Piquero, T.; David, P.; Parmentier, J.; Vix-Guterl, C. The influence of textural properties on the adsorption of hydrogen on ordered nanostructured carbons. *Microporous Mesoporous Mater.* **2005**, *79*, 121–128. [CrossRef]
31. Pevida, C.; Centeno, T.A. Influencia de las propiedades texturales en el almacenamiento de H_2. In *La Energía del Hidrógeno*; Laborde, M.A., Rubiera, F., Eds.; Ediciones CYTED: Buenos Aires, Argentina, 2010; pp. 135–143.
32. Ruthven, D.M. *Principles of Adsorption and Adsorption Processes*; John Wiley & Sons: New York, NY, USA, 1984.
33. Ahmadpour, A.; Wang, K.; Do, D.D. Comparison of models on the prediction of binary equilibrium data of activated carbons. *AIChE J.* **1998**, *44*, 740–752. [CrossRef]
34. Rudziński, W.; Nieszporek, K.; Moon, H.; Rhee, H.-K. On the theoretical origin and applicability of the potential theory approach to predict mixed-gas adsorption on solid surfaces from single-gas adsorption isotherms. *Chem. Eng. Sci.* **1995**, *50*, 2641–2660. [CrossRef]
35. García, S.; Pis, J.J.; Rubiera, F.; Pevida, C. Predicting mixed-gas adsorption equilibria on activated carbon for precombustion CO_2 capture. *Langmuir* **2013**, *29*, 6042–6052. [CrossRef] [PubMed]
36. Álvarez-Gutiérrez, N.; Gil, M.V.; Rubiera, F.; Pevida, C. Adsorption performance indicators for the CO_2/CH_4 separation: Application to biomass-based activated carbons. *Fuel Process. Technol.* **2016**, *142*, 361–369. [CrossRef]

© 2016 by the authors; licensee MDPI, Basel, Switzerland. This article is an open access article distributed under the terms and conditions of the Creative Commons by Attribution (CC-BY) license (http://creativecommons.org/licenses/by/4.0/).